Micromixing of Miscible Liquids in Segmented Gas–Liquid Flow

5 AUTHORS, INCLUDING:

Axel Guenther
University of Toronto

67 PUBLICATIONS **2,741** CITATIONS

Micromixing of Miscible Liquids in Segmented Gas−Liquid Flow

Axel Günther,† Manish Jhunjhunwala,† Martina Thalmann,†
Martin A. Schmidt,‡ and Klavs F. Jensen*,†

*Department of Chemical Engineering and Microsystems Technology Laboratories,
Massachusetts Institute of Technology, Cambridge, Massachusetts 02139*

Ⓦ **This paper contains enhanced objects available on the Internet at http://pubs.acs.org/
journals/langd5.**

We present an integrated microfluidic system that achieves efficient mixing between two miscible liquid streams by introducing a gas phase, forming a segmented gas−liquid (slug) flow, and completely separating the mixed liquid and gas streams in a planar capillary separator. The recirculation motion associated with segmented flow enhances advection in straight microchannels without requiring additional fabrication steps. Instantaneous velocity fields are quantified by microscopic particle image velocimetry (*μ*PIV). Velocities in the direction normal to the channel amount to approximately 30% of the bulk liquid velocity inside a liquid segment. This value depends only weakly on the length of a liquid segment. Spatial concentration fields and the extent of mixing (EOM) are obtained from pulsed-laser fluorescence microscopy and confocal scanning microscopy measurements. The mixing length is reduced 2−3-fold in comparison with previously reported chaotic micromixers that use three-dimensional microchannel networks or patterned walls. Segmented gas−liquid microflows allow mixing times to be varied over several orders of magnitude between milliseconds and second time scales.

1. Introduction

The large time scales associated with transport by diffusion in laminar streams of miscible liquids in microfluidic systems drive the need for schemes that enhance mixing.[1] In addition to mixing enhancement, a residence time distribution narrower than that achievable in single-phase laminar flows is often required. Improved mixing and residence time characteristics are particularly important at high Peclet numbers, that is, when advection dominates over diffusion. Examples are synthesis of nanoparticles in microfluidic devices, biochemical analysis, drug delivery, cell activation, enzyme reactions, and protein folding.

Previous approaches to improve mixing between miscible liquid streams characterized by microscale flows at Peclet numbers between 10^3 and 10^5 have been based on lamination;[2−4] introducing chaotic advection through patterned channel walls,[5,6] or mixing through three-dimensional channel networks.[7] The Peclet number is defined as $\bar{U}d_h/D$, where $\bar{U}$ is the average velocity of the liquid, d_h is a characteristic dimension (the hydraulic diameter), and D is the diffusion coefficient. The fabrica-tion of such mixers generally requires additional processing steps, and the increased channel wall area associated with surface profiling and 3D networks increases the potential for the deposition of solid particles or cells. Flows in most passive micromixers are steady, but enhanced mixing would be expected in transient systems. Recently, active concepts have been presented based on cross-flow,[8] ultrasonic, acoustic,[9] and electrical actuation.[10] Ismagilov et al.[11−13] have presented micromixers based on mixing multiple fluids confined inside liquid droplets dispersed in an immiscible liquid. In this case, the recirculation within the liquid drops provided for the mixing. Relatively high liquid velocities are required to achieve uniform droplet production, which makes this type of mixer attractive for fast reactions.

We present a new mixer design for miscible liquids that is based on segmented gas−liquid (slug) flow. It can be operated over a very large range of liquid flow rates and is therefore compatible with the timescales required for rapid gas−liquid reactions (e.g., direct fluorination), as well as with slow nucleation and nanoparticle growth (quantum dot and sol−gel synthesis). After mixing is accomplished, the gas phase is removed in an integrated gas−liquid separator based on differences in interfacial forces. The resulting outlet streams from the device are consequently single-phase. Section 2 describes the fabrication of different characterization devices that are

* Corresponding author. Phone: (617) 253-4589. Fax: (617) 258-8224. E-mail: kfjensen@mit.edu.
† Department of Chemical Engineering.
‡ Microsystems Technology Laboratories.

(1) Stone, H. A.; Stroock, A. D.; Ajdari, A. *Annu. Rev. Fluid Mech.* **2004,** *36,* 381−411.
(2) Floyd, T. M. Ph.D. Thesis, Massachusetts Institute of Technology, Cambridge, 2001.
(3) Ehrfeld, W.; Golbig, K.; Hessel, V.; Lowe, H.; Richter, T. *Ind. Eng. Chem. Res.* **1999,** *38,* 1075−1082.
(4) Schwesinger, N.; Frank, T.; Wurmus, H. *J. Micromech. Microeng.* **1996,** *6,* 99−102.
(5) Johnson, T. J.; Ross, D.; Locascio, L. E. *Anal. Chem.* **2002,** *74,* 45−51.
(6) Stroock, A. D.; Dertinger, S. K. W.; Ajdari, A.; Mezic, I.; Stone, H. A.; Whitesides, G. M. *Science* **2002,** *295,* 647−651.
(7) Liu, R. H.; Stremler, M. A.; Sharp, K. V.; Olsen, M. G.; Santiago, J. G.; Adrian, R. J.; Aref, H.; Beebe, D. J. *J. Microelectromech. Syst.* **2000,** *9,* 190−197.

(8) Bottausci, F.; Mezic, I.; Meinhart, C. D.; Cardonne, C. *Philos. Trans. R. Soc. London, Ser. A* **2004,** *362,* 1001−1018.
(9) Zhang, L.; Koo, J. M.; Jiang, L.; Asheghi, M.; Goodson, K. E.; Santiago, J. G.; Kenny, T. W. *J. Microelectromech. Syst.* **2002,** *11,* 12−19.
(10) Oddy, M. H.; Santiago, J. G.; Mikkelsen, J. C. *Anal. Chem.* **2001,** *73,* 5822−5832.
(11) Song, H.; Tice, J. D.; Ismagilov, R. F. *Angew. Chem., Int. Ed.* **2003,** *42,* 768−772.
(12) Tice, J. D.; Song, H.; Lyon, A. D.; Ismagilov, R. F. *Langmuir* **2003,** *19,* 9127−9133.
(13) Brinker, C. J.; Scherer, G. W. *Sol−Gel Science: The physics and chemistry of Sol−Gel Processing*; Academic Press: Boston, 1990.
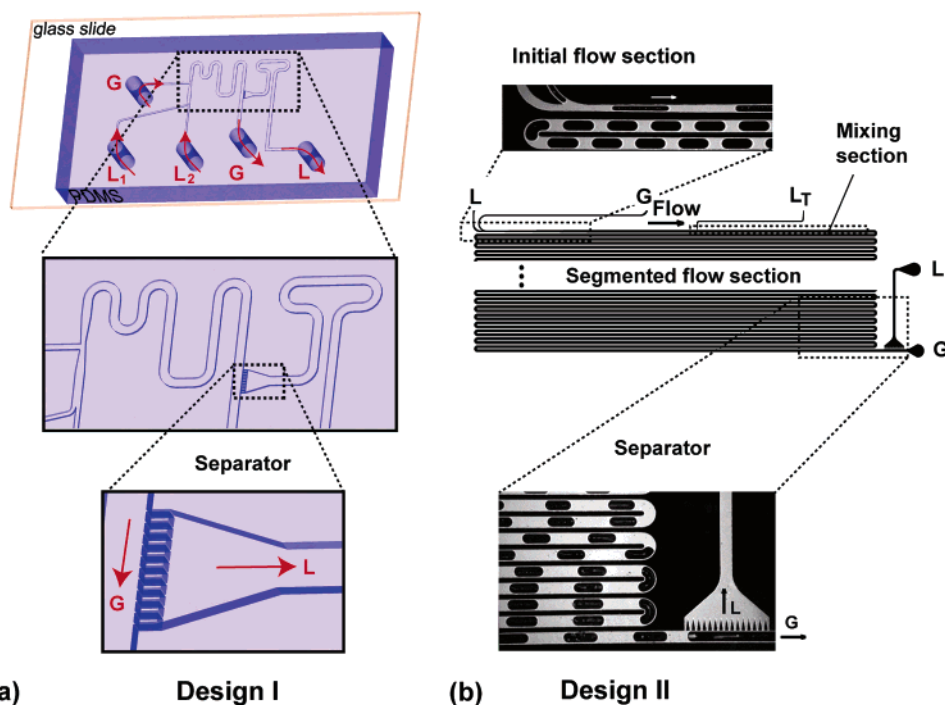
Figure 1. PDMS-based microfluidic devices for mixing studies in segmented gas (G)−liquid (L) flow. (a) Design I: $w = 400$ μm wide and 150 μm deep microchannel. (b) Design II: 400 μm wide and approximately 300 μm deep channel. The length of the segmented flow section was varied between 100 w and 4600 w. In both designs, a capillary phase separator was integrated at the end of the segmented flow section.

formed in poly(dimethylsiloxane) (PDMS) capped with a glass layer, and the experimental setup. Section 3 illustrates the mixing principle and separation of gas from liquid in the capillary separator. Microscale segmented flows in straight and meandering channels are characterized in section 4, including μPIV of recirculation flows in liquid segments. In section 5, we present a scanning confocal microscopy procedure for quantifying the extent of mixing (EOM) from the instantaneous concentration fields at different streamwise positions and flow conditions.

2. Experimental Methods

Microfluidic Devices. To characterize mixing enhancement in segmented flow, we consider microfluidic devices with separate inlets for the two liquid phases, an inlet for an inert gas stream, a mixing section in which the segmented gas−liquid flow is formed, a gas−liquid separator, and outflow ports for the gas and mixed liquids (see Figure 1).

Design I (Figure 1) illustrates the mixing principle. Two liquid inlets, L_1 and L_2, lead into a 400 μm wide (w) and 150 μm deep microchannel, and a gas stream (G) can be injected sidewise. At a location 70 channel widths (28 mm) downstream, a separator parts the gas stream from the liquid. The liquid is drawn from one side of the flow channel through 16 capillaries, each one approximately 20 μm wide.

Microfluidic devices with a substantially larger channel length, design II (Figure 1b), are used to further characterize gas−liquid flow for different gas and liquid segment lengths and to quantify the extent of mixing. All channel features are 290 μm deep. Gas and liquid streams, G and L, are introduced from separate inlets and pass a pressure drop zone before they meet at a 200 μm wide section and form a segmented gas−liquid flow. The top section of Figure 1b shows a typical fluorescence micrograph of the inflow section at gas and liquid flow rates of 30 and 10 μL/min, respectively. The channel is then gradually expanded to its full width of 400 μm, corresponding to a hydraulic diameter, $d_h = 2[w^{-1} + d^{-1}]^{-1}$, of 340 μm. Further downstream, a stream of tracer liquid, L_T, is introduced into the developed gas−liquid flow through a 20 μm wide side inlet that is located a distance

of 80 widths (32 mm) downstream of the location at which the gas−liquid flow is being formed (Figure 1b).

The channel networks for design II had different lengths, depending on the chosen flow conditions, in particular pressure drops. A 4600 widths (1845 mm) long microchannel network consisting of 31 straight segments connected through 180° turns was used for conditions at low gas and liquid flow rates; for example, $G = 30$ μL/min, $L = 10$ μL/min corresponded to liquid phase residence times of approximately 10 min and provided sufficient pressure drop to stabilize the flow. At higher flow rates, for example, $G = 400$ μL/min, $L = 100$ μL/min, shorter channel lengths of 100 widths (34 mm) were sufficient to obtain stable flow conditions. The associated liquid-phase residence times were below 1 s.

Fabrication. Both devices were fabricated in polydimethylsiloxane (PDMS) from a single mask by using standard soft-lithographic techniques.[14] PDMS (Dow Corning Sylgard Brand 184 Silicone Elastomer, Essex-Brownell Inc.) was molded on masters fabricated on silicon wafers using SU-8 (50) (Negative photoresist, Microchem Corp.o, MA). Typically, a single layer of 150 μm thick SU-8 film (design I) or two layers (device II) were spun on 100 mm diameter silicon wafers (Silicon Quest International). Photolithography was used to define negative images of the microfluidic channels, and the wafers were developed using SU-8 Developer (Microchem Corp.). Packaging of the PDMS-based devices was accomplished by molding PDMS on the SU-8 masters at 70 °C for 4−12 h. The devices were then peeled off the mold, cut, and cleaned. Inlet and outlet holes (1/16-in. o.d.) were punched into the material. Individual devices were sealed to precleaned microscope slides (25 × 75 mm, 1 mm thick, VWR Scientific Inc.) Both surfaces were activated in an oxygen plasma (Harrick Co., PDC-32G) for 45 s prior to sealing. PEEK tubing (1/16-in. o.d., 508 μm i.d., Upchurch Scientific) was inserted in the inlet and outlet holes, and was glued in place with 5-min epoxy (Devcon). The epoxy was cured at 70 °C for at least 12 h, prior to use. Outlet tubes were 30 mm long, corresponding to a volume of 6.1 μL. Gas and liquid were delivered separately by syringe pumps (Harvard Apparatus PHD2000). Flow and mixing were characterized using a pulsed-laser fluorescence microscopy and confocal scanning microscopy.

(14) Xia, Y. N.; Whitesides, G. M. *Annu. Rev. Mater. Sci.* **1998**, *28*, 153−184.
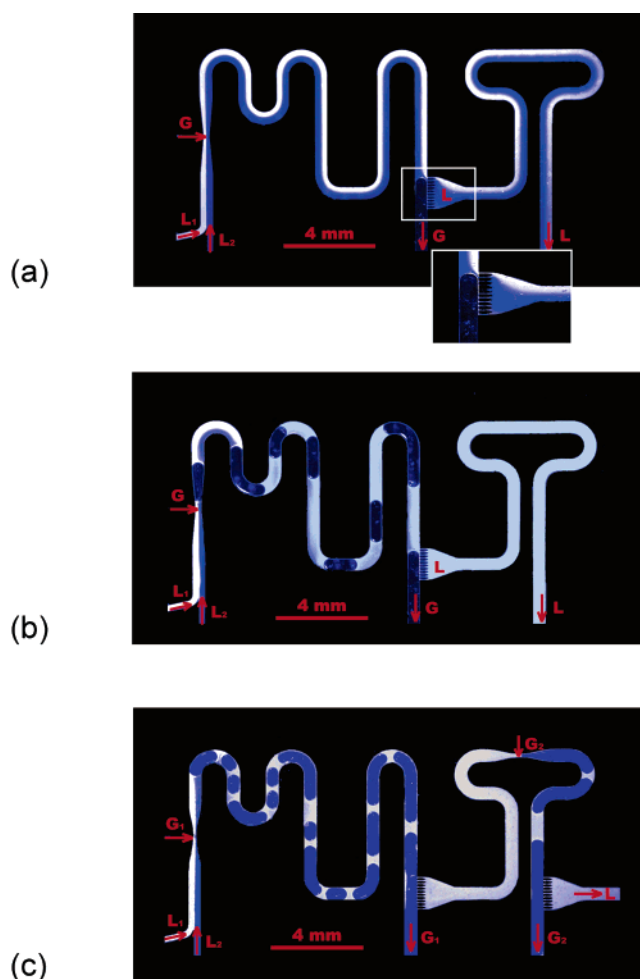
Pulsed Laser Fluorescence Microscopy and Particle Image Velocimetry. An inverted fluorescence microscope (Zeiss Axiovert 200) equipped with a Rhodamine filter set and with a dual-frame CCD camera (PCO QE double shot, 9 frames per second, 1375 × 1039 pixels) was used for imaging. A frequency-doubled Nd:YAG laser (BigSky Ultra CFR, 30 mJ, 532 nm) provided the light source. The two camera frames and the lasers were synchronized using a commercial LaVision timing unit and allowed pulsed-laser fluorescence microscopy measurements of fluorescently labeled liquids. Alternatively, microscopic particle image velocimetry (μPIV) measurements were used to quantify the recirculation motion associated with segmented ethanol−air flows. Ethanol was seeded with 1.0 μm fluorescent particles (carboxylate-modified polystyrene beads containing Nile red, Molecular Probes), and a typical value for the temporal separation between two image frames was 100 μs (the jitter of the lasers is <2 μs). Velocity vector fields were obtained by locally cross-correlating between the two image frames.[15]

Confocal Microscopy. The extent of mixing (EOM) was quantified using a laser scanning confocal microscope (Zeiss LSM 510) with a 10× air objective (numerical aperture: 0.45), where the 488 nm argon line was used as the excitation wavelength. The flow was assumed axisymmetric, and the field of view (880 × 880 μm) consisted of a 5 μm thick optical slice that is located in the center of the microchannel and represented by 512 × 512 pixels in the image plane. Sets of 200 planar confocal scans are typically obtained at different downstream distances from the gas inlet. Two ethanol streams (in the above PDMS device design II) were fluorescently labeled with 10-fold different concentrations of Rhodamine B (diffusivity 2.8 × 10^{-10} m^2/s).

3. Microscale Segmented Flow and Phase Separation

The present mixing strategy takes advantage of the recirculation motion associated with segmented gas−liquid flow in combination with an integrated phase separator. Before discussing the separator operation and quantifying mixing enhancement, we illustrate the mixing scheme with the microfluidic network shown in Figure 1a (design I). Two ethanol streams, L_1 and L_2 (both 5 μL/min), containing 10-fold different concentrations of a fluorescent dye (Rhodamine B) enter the microchannel. In the case where no gas is fed into the channel network ($G = 0$), that is, mixing by liquid-phase diffusion (Figure 2a), the required mixing lengths (>1 m) are substantially longer than the channel length provided. The liquid streams are consequently unmixed even after passing the separator and flowing to the outlet. Note that the liquid is removed from the gas−liquid separator even in the absence of gas injection. When gas is introduced ($G = 30$ μL/min), both liquid streams are efficiently mixed by the recirculation motion associated with segmented gas−liquid flow (Figure 2b). Moreover, the mixed liquid is completely separated from the gas. The design can be further expanded to a two-stage version of the mixer−separator combination (Figure 2c), which creates opportunities for multistage synthesis in multiphase microchemical systems.

Separation is achieved in the capillary separator at the end of the segmented flow channel by applying a differential pressure smaller than the capillary pressure (~0.072 atm for water and ~0.022 atm for ethanol) across the capillary microchannel structure (Figure 3a). The capacity of the separator is governed by the number of capillaries, their cross sections, and lengths. The present design is sufficient to remove liquid from the segmented gas−liquid flows; only gas remains in the main channel. Hence, a complete phase separation is achieved independent of the flow regime as long as the applied pressure

(15) Santiago, J. G.; Wereley, S. T.; Meinhart, C. D.; Beebe, D. J.; Adrian, R. J. *Exp. Fluids* **1998**, *25*, 316−319.

Figure 2. Fluorescence micrographs of mixing between two ethanol streams (L_1 and L_2, 5 μL/min each) in design I. (a) Mixing by diffusion only (no gas flow inserted), (b) an inserted gas stream ($G = 30$ μL/min) creates a segmented gas−liquid flow, and the mixed liquid is removed by the capillary separator, and (c) two-stage operation with two capillary separators.

differential does not exceed the capillary rise pressure in the individual capillaries and the flow rates are below the design limit.

Figure 3b shows the operating conditions of one single capillary and all 16 capillaries contained in the separator for the separation of an ethanol−air mixture. The upper limit of the shaded operating regime is given by the capillary pressure ($\Delta p_c \approx 2\sigma/h$, where the distance h is 20 μm) and applies to all capillaries. The second limit is dictated by the maximum possible flow rate through the capillaries for a given pressure drop below Δp_c. The fluorescence micrographs in Figure 3c illustrate the complete separation of a segmented gas−liquid flow. A differential pressure that is smaller than Δp_c is applied between the outlets of the single-phase gas and liquid streams to accomplish separation (Figure 3b). The gas and liquid flow rates of 16 and 4 μL/min resemble typical conditions for on-chip particle synthesis. Figure 3c also illustrates how the separator adjusts to varying liquid fractions: Individual capillaries adapt between an "active" mode, in which liquid flows through them, and a "passive" mode, where they are closed by a meniscus. Only the first one or two of the 16 available capillaries are "active"; the remaining ones are "passive". Therefore, operating conditions are far from the design limit, and significantly higher flow rates could be handled by this separator.
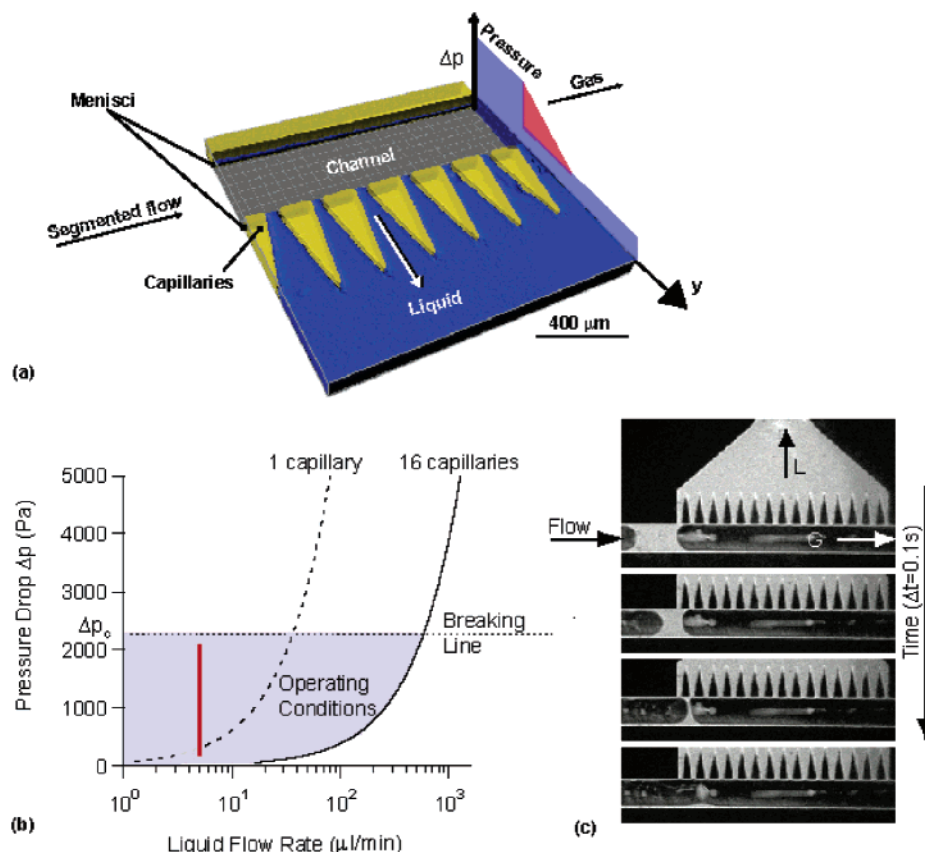
Figure 3. (a) Rendered three-dimensional image of the liquid-filled separator capillaries from confocal microscopy data. Tips of 16 liquid-filled capillaries (20 μm wide) connect to the flow channel and allow the liquid to be removed from the gas−liquid mixture. (b) Liquid separation capacity (shaded areas) for one and for all 16 capillaries calculated for ethanol. The tips of the capillaries have cross sections of 20 μm × 150 μm. (c) Sequence of four fluorescent micrographs demonstrating the complete separation of segmented gas−liquid flow at a flow condition well below the design limit of the separator. Gas and liquid flow rates are 16 and 4 μL/min (operating conditions correspond to the red line in Figure 3b).

4. Characteristics of Microscale Segmented Flows

Introducing a passive gas phase into a liquid stream creates a two-phase flow. Depending on the superficial velocities of the gas, $j_G = V_G/A$, and the liquid, $j_L = V_L/A$, different characteristic flow regimes are obtained. Symbols V_G and V_L are the volumetric flow rates, respectively, and A is the cross-sectional area of the flow channel. Regime diagrams of annular, plug/slug, bubbly, and churn flows have previously been established for gas−liquid flow through conventionally machined[16,17] and microfabricated channels.[18] Figure 4 shows flow regimes as well as the transition line between segmented (plug/slug and bubbly flow regimes) and annular flow regimes. The transition line was established for ethanol/nitrogen and acetonitrile/nitrogen flows through a triangular microchannel ($d_h = 224$ μm). This transition line has also been determined to hold for the ethanol/nitrogen flows and PDMS rectangular channels considered in the present study. Two different regions in the regime diagram are of particular interest as operating conditions for multiphase microchemical systems. Superficial liquid velocities, typically between 0.001 and 0.01 m/s, are similar in both cases, whereas the superficial gas velocities differ. Gas−liquid chemical reactions are typically conducted at high superficial gas velocities, the gray-shaded region in Figure 4a, that is,

close to the flow regime transition line. The flows consist of long gas bubbles (plugs) that are only occasionally interrupted by liquid slugs. The presence of liquid slugs prevents the microchannel side walls from drying.[18] The blue-shaded region identifies conditions where a gas stream is introduced into a co-stream of liquids to enhance mixing and narrow the liquid phase residence time distribution in the otherwise parabolic laminar flow profile. The introduced gas stream forms a train of short liquid and gas segments where the segment length can be controlled through the gas and liquid flow rates (Figure 3b). Short mixing times and narrow residence time distributions require short and uniformly distributed lengths of liquid segments. Such flows are obtained by the gradual expansion of the inflow section (design II). Achieving short slug lengths is important for liquid-phase chemical microreactors because mixing time and slug lengths affect the reaction yield and, in case of particle synthesis, the mean particle size and the size distribution.

Figure 4b shows fluorescence micrographs (design II) of the regularly sized gas and liquid segments for the small superficial gas velocities associated with the blue-shaded region in Figure 4. Obtaining the highly regular flow patterns requires an initial stabilization time (~20 min). In contrast to the gray-shaded regime (Figure 4a) where initial coalescence takes place, a uniform flow pattern is found from the point of gas introduction, and coalescence of initially formed gas bubbles does not occur.

Pulsed-laser fluorescence microscopy of the spatial propagation of the gas−liquid interfaces between two subsequent image frames provides measurements of the

(16) Zhao, B.; Moore, J. S.; Beebe, D. J. *Science* **2001**, *291*, 1023−1026.

(17) Zhao, T. S.; Bi, Q. C. *Int. J. Multiphase Flow* **2001**, *27*, 765−782.

(18) de Mas, N.; Guenther, A.; Schmidt, M. A.; Jensen, K. F. *Ind. Eng. Chem. Res.* **2003**, *42*, 698−710.
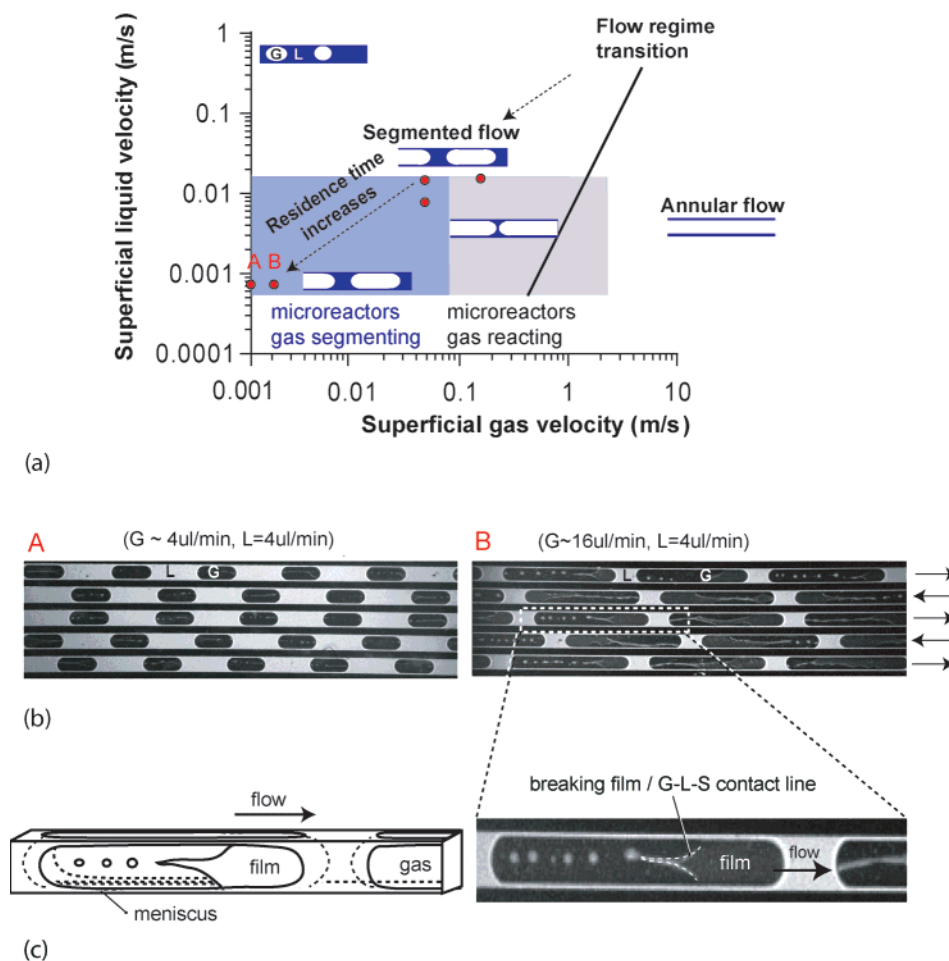
Figure 4. (a) Regime diagram for gas−liquid flow in microchannels (design II) indicating the transition line between segmented and annular flow.[18] For ethanol, acetonitrile, or hexane as the liquid phase and triangular and rectangular channel cross sections, the transition line can be approximated as $j_L = 0.00606(j_G)^{2.855}$ (superficial velocities in m/s) for hydraulic diameters between 224 and 433 μm. Conditions for mixing in segmented flow are $j_G = 1.2$ mm/s to 180 mm/s, $j_L = 0.6$ mm/s to 9 mm/s (circles). (b) Fluorescence micrographs of segmented ethanol−air flows at two different flow conditions with large residence times. Scale bars correspond to 50 μm. (c) Fluorescence micrograph of breaking liquid film for segmented flow through straight channels.

bubble velocity, U_b, and, correspondingly, the Capillary number $Ca = \mu U_b/\sigma$ (σ denotes the surface tension). From a series of fluorescent images, the void fraction $\epsilon = V_G/(V_G + V_L)$ can be estimated. The average velocity of the liquid phase in the channel then follows as $U_L = j_L/(1 - \epsilon)$, and the average residence time for a given length of the microchannel, Λ, is then $E \approx \Lambda(1 - \epsilon)/j_L$. Taylor[19] predicted internal recirculation for values of $m = (U_b - U_{bulk})/U_b < 0.5$, that is, for a moderate slip between the liquid and the gas phases, where U_{bulk} is the bulk liquid velocity in the liquid segment. The value for m is smaller than 0.02 for the considered Capillary number ranges.[20]

The instantaneous velocity field inside a liquid segment (Figure 5) is determined by cross-correlating two subsequent fluorescence images of a particle seeded ethanol−nitrogen flow. The velocity field reveals the recirculation motion and a stagnation point close to the channel center. The maximum velocity in the direction normal to the channel is approximately 30% of the average liquid velocity (U_{bulk}) in the channel. A contour plot of the vorticity distribution, $\partial U/\partial y + \partial V/\partial x$ (Figure 5e), is a further indication of the mixing potential of segmented gas−liquid flows. Large local vorticity gradients are indicative of mixing enhancement inside the liquid segments.

The quantities in Figure 5b−e are obtained from the same image pair. Even though the mixing mechanism can be well illustrated for single instantaneous images, distributions of the obtained quantities across a set of images are better representations of the temporal behavior (or uniformity) of the segmented flow. As an example, Figure 5f shows the distribution of liquid slug lengths across 200 image pairs acquired at a frame rate of approximately 3 Hz.

Flow Symmetry. Microchannel design II (Figure 1b) was also used to explore effects of channel geometry on the symmetry of the flow field. Specifically, two different microchannel configurations with the same cross-sectional area (400 μm wide and 300 μm deep) were considered: (i) a straight channel consisting of two parallel side walls, and (ii) a meandering channel with the same mean width and depth. The latter consists of a meandering pattern of alternating half-circles (diameter of the centerline = 1200 μm).

Microscopic PIV data (Figure 6 and Web Enhanced Object) were obtained at a fixed streamwise position, and pulsed-laser microscopy measurements were conducted at three different streamwise distances from the gas inlet ($0d_h$, $13d_h$, and $26d_h$). For straight channels (Figure 6a) and the low flow rates considered, most instantaneous velocity fields in the liquid phase deviate

(19) Taylor, G. I. *Proc. R. Soc. London, Ser. A* **1953**, *219*, 186−203.
(20) Wong, H.; Radke, C. J.; Morris, S. *J. Fluid Mech.* **1995**, *292*, 71−94.
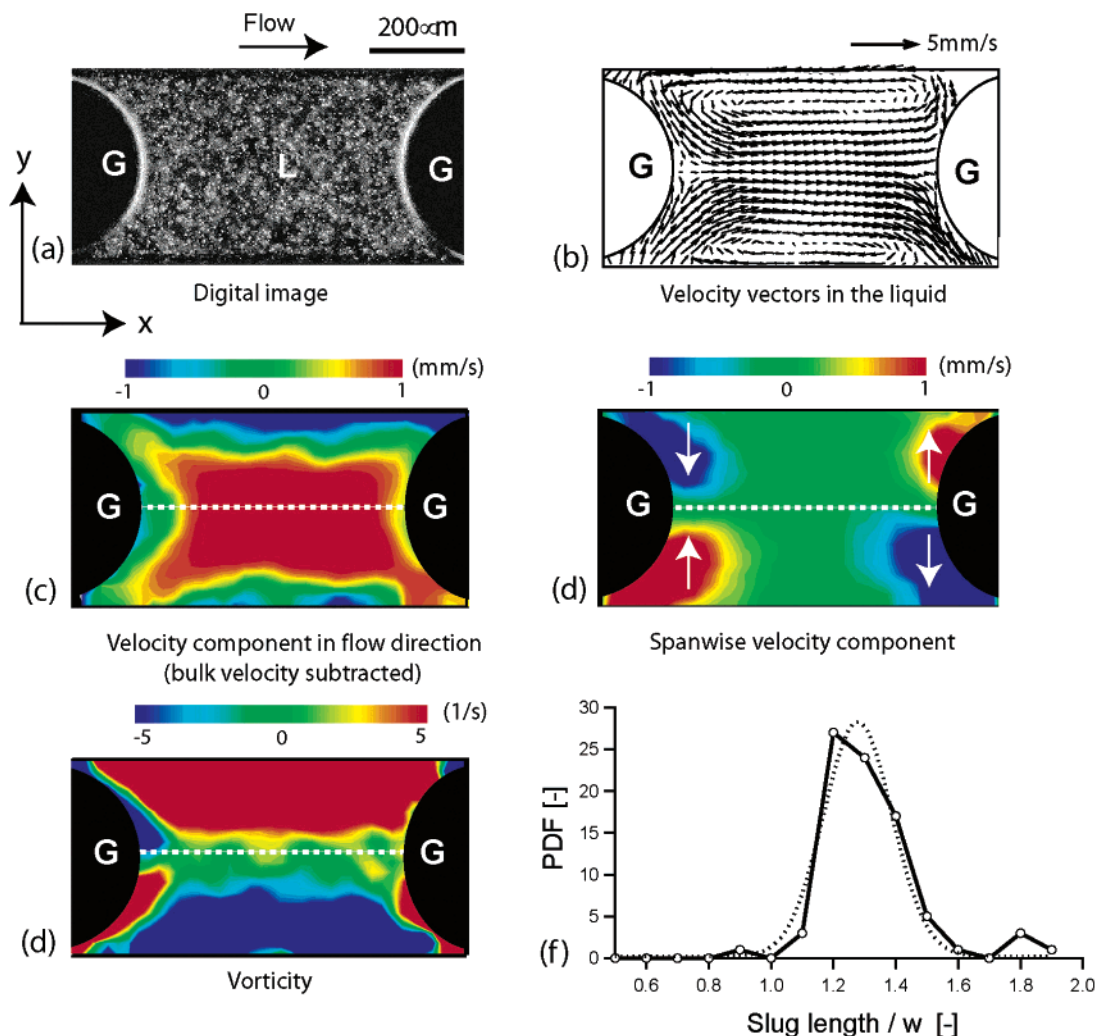
Figure 5. (a) Instantaneous fluorescence micrograph of an ethanol segment between two air bubbles in the 400 μm wide channel seeded with fluorescent polystyrene particles (diameter 1 μm) for developed flow (gas flow rate, 30 μL/min; liquid flow rate, 10 μL/min). (b) The velocity vector field, (c) the contours of the streamwise velocity component, (d) the normal velocity component, and (e) the vorticity $\partial U/\partial y + \partial V/\partial x$ are obtained from image pairs using a cross correlation PIV algorithm. Note that $U_{bulk} = 5.5$ mm/s was subtracted in all velocity plots. (f) Slug length distribution for gas and liquid flow rates of 30 and 10 μL/min.

slightly from ideal center plane symmetry flow fields. We attribute this effect to the breaking of the thin liquid films at the side walls (Figure 4c). The breaking films create a gas–liquid–solid contact line moves alongside the microscopically rough side walls. The roughness is caused by the limited resolution of the transparency masks used in the lithography process. The randomness of the surface roughness causes the asymmetry of the gas–liquid interfaces at the leading and trailing ends of bubbles, and hence small asymmetry of the velocity field inside liquid segments. Such symmetry deviations are not observed for segmented liquid–liquid flows at sufficiently high superficial velocities,[21] where both fluids are incompressible and the dispersed phase is in no direct contact with the channel walls. Asymmetry of the flow field, which results in transport across the channel centerline, is desirable to achieve efficient mixing not only within the two channel halves (due to recirculation) but also across the entire channel. As expected, the asymmetry is significantly increased in meandering channels (Figure 6c).

## 5. Quantification of Mixing in Microscale Segmented Flow

This section quantitatively describes mixing in segmented flow. For the mathematical foundations of mixing in microfluidic systems, we refer to Aref[22] and a recent review by Wiggins et al.[23] To quantify microfluidic mixers that involve steady flows,[5–7] the spatial distribution of a tracer dye is commonly determined by confocal microscopy and the spatial variation of the tracer concentration. Confocal microscopy offers the advantage of successively assessing local tracer concentrations within thin optical slices. Segmented flows, however, are transient, which implies that only local instantaneous concentration fields are physically meaningful and imposes requirements on the temporal measurement resolution. Time-averaged concentration fields that are justified under steady flow conditions have also been applied for determining the EOM in segmented flows.[11] We demonstrate that, in transient flow cases, mixing lengths can be slightly underestimated if they are determined from time average data. One reason for choosing time average (steady state) data is that time-resolved local concentrations are more difficult to obtain.

(21) Ismagilov, R. F.; Stroock, A. D.; Kenis, P. J. A.; Whitesides, G.; Stone, H. A. *Appl. Phys. Lett.* **2000**, *76*, 2376–2378.

(22) Aref, H. *J. Fluid Mech.* **1984**, *143*, 1–21.
(23) Wiggins, S.; Ottino, J. M. *Philos. Trans. R. Soc. London, Ser. A* **2004**, *362*, 937–970.
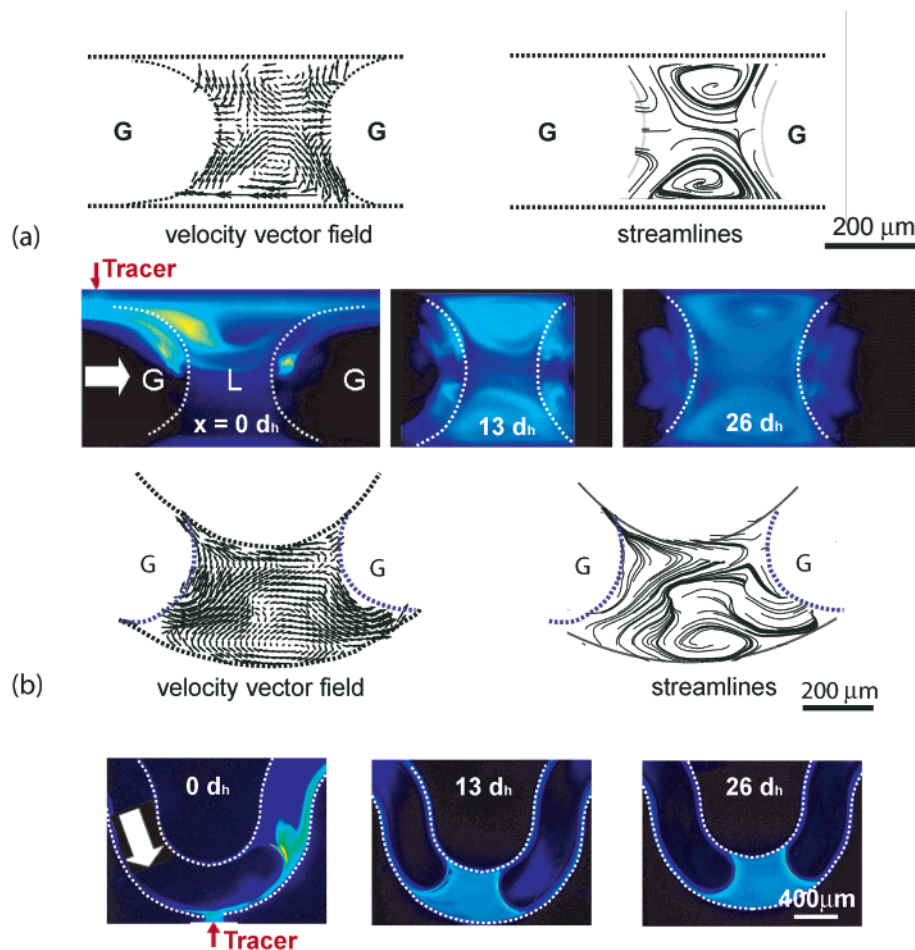
Figure 6. Velocity and concentration fields for segmented flow through straight (a) and (b) meandering microchannels (width 400 μm, depth 280 μm). Instantaneous velocity vector and streamline plots are obtained from μPIV measurements, and concentration fields are measured using pulsed-laser fluorescence microscopy. Gas and liquid flow rates are $G = 30$ μL/min and $L = 10$ μL/min.

Ⓦ A movie clip in AVI format is available.

We consider design II, where a tracer stream (Rhodamine B) is sidewise injected into a developed gas−liquid flow. The tracer concentration in the injected stream is 10-fold higher than the original concentration in the liquid phase (ethanol), and its flow rate is 10-fold smaller. The considered liquid segments are approximately 1.2 channel widths (w) long (Figure 5f). We apply confocal scanning microscopy to segmented gas−liquid flow at bubble velocities, U_B, between approximately 5 and 100 mm/s. At a channel depth (z) corresponding to the channel center, sets of 200 planar confocal scans are obtained at different downstream distances (x), 13 w, 26 w, 39 w, and 52 w, from the point of tracer injection. The fluorescent signal locally emitted from the liquid phase is characterized by a high intensity and can therefore be distinguished from the gas phase (low intensity). Figure 7a schematically illustrates the gas−liquid distribution for such a system that would be obtained from scanning through an (x,y)-plane a z-location that corresponds to the channel center with unidirectional line scans; that is, the fluorescence signal is only collected in one direction (marked as a red arrow in Figure 7a), and not on the returning path (blue). The time required for scanning one pixel (t_{scan}) can be chosen between 0.72 and 287 μs. At the low limit, a higher amplifier-gain is required which increases the electronic noise of the photomultiplier tube (PMT) and reduces the signal-to-noise ratio (SNR). At the upper limit, the scan is substantially slower, reducing the necessary amplifier gain, and therefore the electronic noise contribution.

However, the larger sampling time also leads to undesired streamwise averaging at the pixel level. We require the distance a fluid element travels during t_{scan} to be smaller than the spatial pixel resolution for the 10× objective, 1.76 μm. To increase the SNR (decrease PMT noise), t_{scan} = 3.2 μs is chosen so that (assuming a liquid velocity $O\{U_b\}$) a fluid element travels a distance during this scan time of 0.0375 μm ≪ 1.76 μm. Scanning the entire plane is too slow to "freeze" the instantaneous spatial distribution of gas and liquid (a full scan requires 3.5 s). Nevertheless, an accurate measurement of EOM can be determined by choosing t_{scan} sufficiently large to prevent averaging on the pixel level and performing signal processing of the collected pixel level information.

Signal Processing. We calculate statistical quantities in the (x,y)-plane from the intensity information obtained from a large enough set of statistically independent planar scans that are stored as digital image files (Figure 7b) with 488 nm as the excitation wavelength. The figures show the spatial intensity distributions. The thickness of the slice is 5 μm. For each pixel, the image intensity is collected at a photomultiplier tube during a scanning time of only t_{scan} = 3.2 μs. One planar scan i therefore contains a spatial noise distribution, $I_{i,noise}(x,y)$, that belongs to different instances in time. Figure 7b shows typical examples of the instantaneous intensity distributions for such a scan at three different streamwise locations: at the point of tracer introduction, 13 and 26 widths downstream, respectively. The light intensity detected on the PMTs is
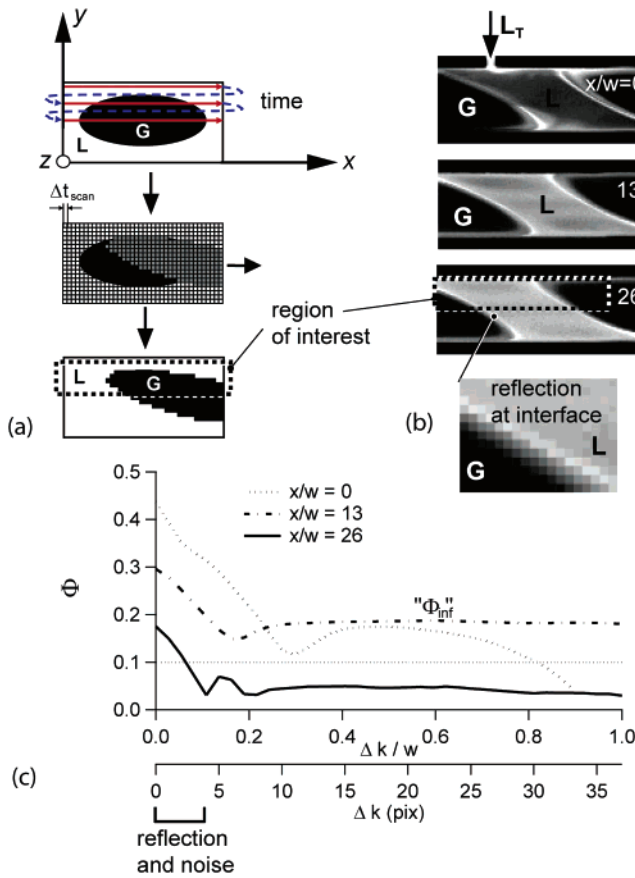
Figure 7. (a) Schematic of a planar scan that consists of unidirectional line scans across a transient gas (G)−liquid (L) flow using a confocal laser scanning microscope (Zeiss LSM 510). Time t_{scan} is required to scan one pixel in the plane ($\delta_z = 5\ \mu$m). (b) Shows a set of subsequently obtained planar scans obtained for three different downstream distances from the location of tracer introduction ($x/d_h = 0, 13, 26$). The gas and liquid superficial velocities for this example are 4.4 and 1.5 mm/s. The planes are located in the center of the 400 μm wide and 280 μm deep microchannel, and the focal plane has a depth, Δz, of 11 μm. (c) Spatial autocorrelation function used to discriminate measurement noise from the signal when determining the EOM from time-resolved confocal scans.

accompanied by electronic noise, for which a Gaussian behavior is assumed so that the average over all frames and validated pixels vanishes, $\langle I_{i,\text{noise}}(x,y)\rangle_{i,x,y} = 0$. For frame i, we obtain $I_{i,\text{meas}}(x,y) = I_i(x,y) + I_{i,\text{noise}}(x,y)$. Only the liquid phase is accounted for, that is, the gas phase excluded by excluding data with intensities below an intensity threshold (20% of the mean intensity of the image). From all validated intensities across frames follows the ensemble average

$$\langle I_{i,\text{noise}}(x,y)\rangle_{i,x,y} = \langle I_{i,\text{meas}}(x,y)\rangle_{i,x,y} = \langle I\rangle \qquad (1)$$

For steady flows, instantaneous and time-averaged intensities only differ by their noise contribution, and time-averaged information can be used to judge upon the degree of mixing.[6,7] We now present the following methodology for determining EOM, that is, mixing lengths and times, for transient flow situations based on the standard deviation of the local and instantaneous fluctuation $I'(x,y) = I(x,y) - \langle I\rangle$ from the spatial average, $\langle I\rangle$, over all frames i:

$$\Phi(\Delta x) = \frac{\langle I'_{i,\text{meas}}(x,y)I'_{i,\text{meas}}(x + \Delta x, y)\rangle^{0.5}}{\langle I\rangle} \qquad (2)$$
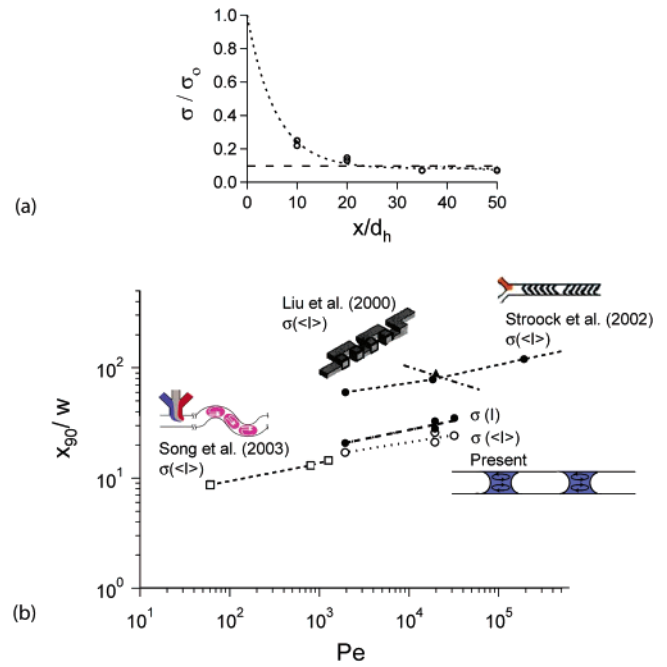
Figure 8. (a) Standard deviation for large Δx, as a function of the downstream location. The intersection with the obtained curve with $\sigma = 0.10$ defines an EOM of 90%. (b) mixing length based on the local and the time-averaged concentration fields obtained in segmented flow at the conditions shown in Figure 2. We compare with literature data for a patterned channel,[6,7] and for a droplet-based mixer with $d_h = 34.5\ \mu$m.[11] For the latter, we used the superficial velocity of the aqueous phase and the diffusion constant 1.9×10^{-9} m^2/s.

where the spatial autocorrelation function contains the measurement noise: $I'_{i,\text{meas}}(x,y) = I'_i(x,y) + I'_{i,\text{noise}}(x,y)$. The autocorrelation function is then calculated from all validated $I'_{i,\text{meas}}(x,y)$ in the x-direction and averaged over the set of images and the y-direction. Unlike the case of calculating the average (eq 1), the noise distribution does not vanish for higher moments, specifically not in eq 2. Signal and noise are assumed to be uncorrelated because the scanning time within one line (fixed y) was sufficiently short:

$$\Phi(\Delta x) = \langle I'_{\text{meas}}(x)I'_{\text{meas}}(x + \Delta x)\rangle$$
$$\approx \langle I'(x)I'(x + \Delta x)\rangle_y + \langle I'_{\text{noise}}(x)I'_{\text{noise}}(x+\Delta x)\rangle_y \qquad (3)$$

Consistent with the assumption of Gaussian noise, we expect the second term at the right side to dominate at $\Delta x = 0$ and to only correlate for small Δx. For larger Δx, its influence decays. The term $\langle I'_{\text{meas}}(x)I'_{\text{meas}}(x + \Delta x)\rangle_y$ can therefore be approximated as $\langle I'(x)I'(x + \Delta x)\rangle_y$, which is then independent of Δx and equal to $\Phi_{\text{inf}}{}^2\langle I\rangle^2$ for the well-mixed case (Figure 7).

Figure 8a shows the standard deviations σ as a function of the streamwise distance from the location of tracer injection. The superficial gas velocity is a parameter in this plot. For the considered value of $Pe = 2.06 \times 10^4$, a distance of less than $\Delta x/w = 25$ is required for x_{90}. This value is denoted as $\sigma(I)$ in Figure 8b, and compared to literature data for passive micromixers consisting of patterned or three-dimensional microchannel networks,[6,7] and with the droplet-based technique of Song et al.[10] We varied the Peclet number by changing the superficial liquid velocity while adjusting the superficial gas velocity in such a way that short liquid segments with average lengths between 400 and 550 μm and narrow length distributions (<10%) were obtained across all flow conditions. Our

scheme provides 2−3 times shorter mixing lengths as compared to patterned and 3D channels and shows trends similar to those reported by Song et al.[11] for lower *Pe* numbers. In the latter case, the EOM was determined on the basis of the time-averaged fluorescence intensity produced by a chemical reaction.

If we calculate our EOM based on the standard deviation of the time-averaged concentration fields, $\sigma(\langle I \rangle)$ (○ in Figure 8b), the criterion is less restrictive than if we follow our transient analysis (●). Determining EOM from average intensities is likely to overestimate the mixing efficiency. In particular for rapid chemical reactions occurring before complete mixing is accomplished, for example, for precipitation processes, a transient analysis might be necessary.

6. Summary and Conclusions

We have presented a method for efficiently mixing two liquid streams on a microscale by first adding and subsequently removing an inert gas phase. The mixing relies on recirculation in segmented gas−liquid flow in combination with an integrated gas−liquid separator. We have quantified the velocity and concentration fields in the liquid phase during mixing. Confocal scanning microscopy and image processing procedures determined the extent of mixing (EOM) and the mean residence time. For similar Peclet numbers and without requiring additional fabrication steps, the mixing lengths are reduced 2−3-fold as compared to passive mixers with patterned side walls or three-dimensional channel geometries.[6,7]

To demonstrate the simplicity of the integrated mixer, we fabricated a planar version in PDMS, which only requires a single photolithographic mask. A version of the micromixer that is resistant to most solvents, acids, and bases has also been fabricated in silicon by a process requiring three photolithographic masks. The two-stage version of the mixer−separator indicates that the concept can be extended to conducting chemical reactions in segmented flow, and using the single-phase products resulting from the separator in subsequent reaction processes for integrated microchemical systems.